Journal of Computational and Applied Mathematics 382 (2021) 113106

Contents lists available at ScienceDirect

Journal of Computational and Applied Mathematics

journal homepage: www.elsevier.com/locate/cam

Isogeometric analysis of the new integral formula for elastic energy change of heterogeneous materials

D.Y. Sun, C.Y. Dong *

Department of Mechanics, School of Aerospace Engineering, Beijing Institute of Technology, Beijing 100081, China

ARTICLE INFO

Article history:
Received 12 June 2019
Received in revised form 10 July 2020

Keywords:
Isogeometric boundary element method (IGABEM)
Heterogeneous material
Variation of elastic energy
Integral formula

ABSTRACT

In recent years, more and more attention has been paid to isogeometric methods, in which shape functions are used to accurately describe CAD models and approximate unknown fields. The isogeometric boundary element method (IGABEM) realizes the integration on the exact boundary of the region, which means there is no geometric discretization error. In this paper, a more general interface integral formula for elastic energy increment of heterogeneous materials is extended from previous work (Dong, 2018), in which the only unknown variable is the displacement located on the interface between matrix and inclusion. This feature makes it more compatible with boundary element method (BEM) because of none of volume parametrization. However, the geometry discontinuity on the boundary called 'corner point problem' increases the difficulty and decreases the accuracy when solving complex numerical examples when heterogeneous structures are considered. The discontinuous element method combined with IGABEM is presented and applied to deal with 'corner point problem'. In the numerical examples, the interface between matrix and inclusion is discretized by quadratic isogeometric elements. Compared with the analytical solution, the numerical results show that the method has higher accuracy and efficiency.

1. Introduction

Composite materials based on different shapes and material properties have been widely used in science, technology and life areas. The strain energy is an important parameter that can represent the property of composite materials. There are various applications of this special parameter for evaluating the mechanical properties of materials. For martensitic transformations, the rate of transformations will depend on the energy barrier or the strain energy of mixed microstructure of martensite and austenite [1]. Eshelby [2] proposed the analytical solutions for stress field produced by a sphere or ellipsoidal inclusion. However, this formula has less accuracy for inclusions of arbitrary shape and distribution. For numerical methods, Young and Nam [3] derived the new calculation method of elastic strain energy of inclusions from Green's function by finite element method (FEM), in which the plane stress covering the domain should be calculated firstly. Meanwhile, in fracture mechanics, the energy is seen as a criterion or condition for propagation of a crack. Griffith [4,5] introduced the Maximum Energy Release Rate criterion (MERR) which states that crack growth follows the orientation of maximum energy release rate. And the strain energy approach has been used to evaluate the static and fatigue behavior of notched or unnotched components in materials [6]. Boulenouar et al. [7] presented a numerical modeling to predict crack propagation with strain energy density which can be solved by FEM. For the variation of elastic

* Corresponding author.
E-mail address: cydong@bit.edu.cn (C.Y. Dong).

https://doi.org/10.1016/j.cam.2020.113106
0377-0427/

energy of heterogeneous materials, Christensen [8] presented a more efficient interface integral formula to calculate this parameter. Note that, the displacements and tractions on interface between inclusions and matrix rather than whole domain must be calculated firstly in this formula by FEM or BEM. Dong [9] derived a new integral formula to calculate the variation of elastic energy of any arbitrary shape, taking advantage of various elastic properties of materials.

Hughes et al. established the isogeometric analysis method (IGA) [10], which has eliminated the gap between CAD and computer aided engineering (CAE) because of integrating the computational model with design model. This method can accurately simulate complex geometric shapes, not only simplifying the process of mesh refinement, but also maintaining the geometric continuity on the field variables of the design model. Meanwhile, the convergence of numerical solution can be conveniently verified by mesh refinement. Based on the above advantages, the combination of IGA and FEM, known as IGAFEM, has been used to solve many problems, such as structural and vibration analysis [10], shape optimization [11], hydromechanics [12–14], acoustics [15,16], electromagnetism [17,18], biomechanics [19,20] and contact mechanics [21,22]. Meanwhile, in recent years, the combination of IGA and BEM, known as IGABEM, has received more and more attentions for successfully solving elasticity problems [23–25], potential problems [26], fast multipole IGABEM [27,28], Helmholtz problems [29], acoustic problems [30,31], and crack problems [32,33]. The symmetric Galerkin boundary element method (SGBEM) [34] is a weak formulation of BEM, which has superior properties of stability, consistency and convergence compared to collocation method. The combination of IGA and SGBEM has been applied to 2D Laplace problem [35,36], 2D fracture problems [32] and 3D elasticity problems [37] in recent years. However, no matter it is BEM, IGABEM or SGBEM, there are various singular integrals in boundary integral equations, such as weak singularity, strong singularity, and hyper-singularity. At present, there are many efforts to eliminate or decrease the singularity in the boundary integral equations, for examples, the so-called Telles algorithm [38] is self-adaptive and adapts to eliminate the singularity and improves the accuracy of Gauss quadrature rule. The power series expansion method, provided by Gao [39], can be used to calculate various degrees of singular integrals. Those two methods are applied in this paper for solving singularity problems in 2D and 3D, respectively.

The geometry of an arbitrary object can be described accurately by Non-Uniform Rational B-splines (NURBS) basis functions. Once the mesh of geometry is completed, it can be refined and enriched by knot-insertion (h-refinement), degree-elevation (p-refinement) or by k-refinement (high-degree and maximal smoothness) procedures without geometric error [40]. In this paper, we proposed a more general interface integral formula for the variation of the matrix elastic energy of heterogeneous materials, and applied IGABEM to obtain numerical results. In order to deal with corner point problem on heterogeneous structures, discontinuous element method is combined with IGABEM for getting more accurate and reasonable results. The work in this paper can be further extended to the study of inclusion shape optimization and effective mechanical properties of composite materials.

A brief description of this paper is given below. The second section gives the new interface integral formula about the variation of elastic strain energy. Section 3 shows the basic formulas of NURBS basis functions. Section 4 gives the boundary integral equations of IGABEM about heterogeneous structure. Section 5 summarizes the power series expansion method for the strongly and weakly singular integrals. Section 6 provides numerical examples to demonstrate the accuracy and efficiency of the proposed method. Finally, conclusions and future works are proposed in Section 7.

2. Integral formula for the variation of elastic energy

A more general integral formula for the variation of elastic energy has been proposed in [41]. Here are some details about the derivative process. Consider one inclusion of another material embedded into one homogeneous media subjected to the remote loading as Fig. 1. The variation of elastic strain energy of heterogeneous structure due to the existence of inclusion has the following form [8]:

$$\Delta U = \frac{1}{2}\int_{\Gamma}\left(t_i^0 u_i - t_i u_i^0\right) d\Gamma \tag{1}$$

where Γ denotes the interface between the inclusion and matrix, u_i and t_i ($i = 1, 2, 3$ for 3D problems) are the displacement and traction on the interface between the inclusion and matrix, respectively. The repeated indices imply summation. And the symbols with the superscript 0 mean the variables derived from remote loading.

In previous work [9], the same Poisson' s ratio from the inclusion and matrix is assumed in deriving the integral formula, thus the special treat about corner point problem is avoided, such as discontinuous element method. Here, we extend this formulation under different Poisson' s ratios of heterogeneous structure. The detailed derivations are as follows:

The second term on the right hand side of Eq. (1) can be rewritten as

$$\int_{\Gamma} t_i u_i^0 d\Gamma = \int_{\Omega} \sigma_{ij}\varepsilon_{ij}^0 d\Omega \tag{2}$$

where the strain tensor $\varepsilon_{ij}^0 = \frac{1}{2}\left(u_{i,j}^0 + u_{j,i}^0\right)$ in which the tensor $u_{i,j}^0$ is called the displacement gradient tensor. In derivation process of Eq. (2), the equilibrium equation ($\sigma_{ij,j} = 0$) and Green's theorem have been used.

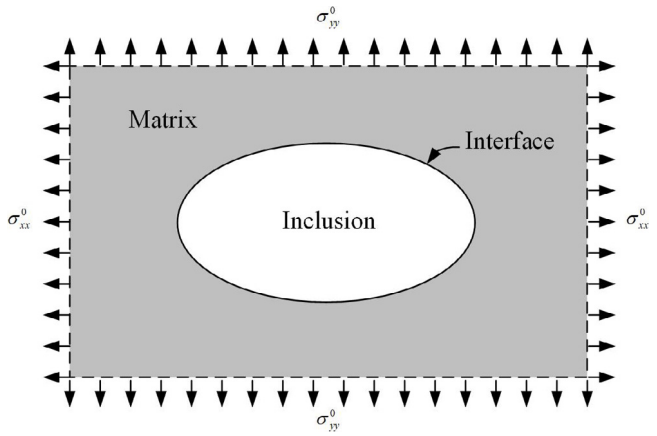

Fig. 1. An inclusion embedded in an infinite anisotropic elastic matrix subjected to remote stresses.

The general 3D constitutive law for linear elastic materials can be expressed in standard tensor notation by the following form [42]

$$\sigma_{ij} = C_{ijkl}\varepsilon_{kl} \tag{3}$$

where C_{ijkl} is a four-order elasticity tensor, and for the isotropic materials, it can be given in the form below

$$C_{ijkl} = \lambda\delta_{ij}\delta_{kl} + G\left(\delta_{ik}\delta_{jl} + \delta_{il}\delta_{jk}\right) \tag{4}$$

where $\lambda = \frac{E\nu}{(1+\nu)(1-2\nu)}$ is called the Lame's constant, and $G = \frac{E}{2(1+\nu)}$ is the shear modulus in which E is called the modulus of elasticity, and ν is referred to as Poisson's ratio.

For the inclusion and matrix, we have

$$C^I_{ijkl} = \lambda^I\delta_{ij}\delta_{kl} + G^I\left(\delta_{ik}\delta_{jl} + \delta_{il}\delta_{jk}\right) \tag{5}$$

and

$$C^M_{ijkl} = \lambda^M\delta_{ij}\delta_{kl} + G^M\left(\delta_{ik}\delta_{jl} + \delta_{il}\delta_{jk}\right) \tag{6}$$

In Eqs. (5) and (6), the superscripts I and M denote the inclusion and matrix, respectively.

By means of Eqs. (5) and (6), one can obtain the relationship between C^I_{ijkl} and C^M_{ijkl}, i.e.

$$C^I_{ijkl} = \frac{(1+\nu_M)E_I}{(1+\nu_I)E_M}C^M_{ijkl} + \frac{(\nu_I-\nu_M)E_I}{(1+\nu_I)(1-2\nu_I)(1-2\nu_M)}\delta_{ij}\delta_{kl} \tag{7}$$

Substituting Eq. (7) into Eq. (3) yields

$$\sigma^I_{ij} = \frac{(1+\nu_M)E_I}{(1+\nu_I)E_M}C^M_{ijkl}\varepsilon_{kl} + \frac{(\nu_I-\nu_M)E_I}{(1+\nu_I)(1-2\nu_I)(1-2\nu_M)}\delta_{ij}\varepsilon_{mm} \tag{8}$$

Thus, the integral on the right-hand side of Eq. (2) becomes

$$\int_\Omega \sigma_{ij}\varepsilon^0_{ij}d\Omega = \frac{E_I}{(1+\nu_I)E_M}\int_\Gamma\left[(1+\nu_M)t^0_k + \frac{(\nu_I-\nu_M)}{(1-2\nu_I)}\sigma^0_{mm}n_k\right]u_k d\Gamma \tag{9}$$

Substituting Eq. (9) back into Eq. (1) produces one simplified formula of the variation of matrix elastic energy for heterogeneous materials as follows:

$$\Delta U = \frac{1}{2}\int_\Gamma\left[\left(1 - \frac{(1+\nu_M)E_I}{(1+\nu_I)E_M}\right)t^0_i - \frac{(\nu_I-\nu_M)E_I}{(1+\nu_I)(1-2\nu_I)E_M}\sigma^0_{mm}n_i\right]u_i d\Gamma \tag{10}$$

where $m = 1, 2, 3$ for 3D problems, and $m = 1, 2$ for plane stress problems. For plane strain problems, Eq. (10) should be modified as

$$\Delta U = \frac{1}{2}\int_\Gamma\left[\left(1 - \frac{(1+\nu_M)E_I}{(1+\nu_I)E_M}\right)t^0_i - \frac{(\nu_I-\nu_M)(1+\nu_M)E_I}{(1+\nu_I)(1-2\nu_I)E_M}\sigma^0_{mm}n_i\right]u_i d\Gamma \tag{11}$$

where $m = 1, 2$.

If the inclusion and matrix have the same Poisson's ratio, i.e. $\nu_I = \nu_M$, then Eq. (11) can be further simplified as [9]

$$\Delta U = \frac{1}{2}\left(1 - \frac{E_I}{E_M}\right)\int_\Gamma t_i^0 u_i d\Gamma \tag{12}$$

Compared with Eq. (1), the only unknowns in Eq. (10) are the displacements that can be conveniently calculated using the BEM [42]. Eqs. (10) and (11) can easily be extended to many inclusions, i.e.

$$\Delta U = \frac{1}{2}\sum_{l=1}^{N}\int_{\Gamma_l}\left[\left(1 - \frac{(1+\nu_M)E_I}{(1+\nu_I)E_M}\right)t_i^0 - \frac{(\nu_I - \nu_M)\,E_I}{(1+\nu_I)(1-2\nu_I)E_M}\sigma_{mm}^0 n_i\right]u_i d\Gamma \tag{13}$$

and

$$\Delta U = \frac{1}{2}\sum_{l=1}^{N}\int_{\Gamma_l}\left[\left(1 - \frac{(1+\nu_M)E_I}{(1+\nu_I)E_M}\right)t_i^0 - \frac{(\nu_I - \nu_M)\,(1+\nu_M)E_I}{(1+\nu_I)(1-2\nu_I)E_M}\sigma_{mm}^0 n_i\right]u_i d\Gamma \tag{14}$$

where N expresses the total number of inclusions. Here, l denotes the lth inclusion. When $E_I = E_M$ and $\nu_I = \nu_M$, i.e. no inclusions, ΔU is equal to zero as expected.

After the interface displacements are obtained by using the subdomain boundary element method [18], the variation of matrix elastic energy of heterogeneous materials can easily be calculated using Eq. (13) or (14).

3. NURBS basis function

In isogeometric analysis, the shape functions that are used to describe the CAD models exactly are also the same functions that are used to approximate the unknown fields in the numerical analysis [43]. In this paper, the basic implementations about NURBS in the IGABEM are introduced [25,43], thus we can get any shape inclusions through NURBS.

To define fully a NURBS, the following four items are first required.

- The curve degree p, e.g. linear ($p = 1$), quadratic ($p = 2$).
- A set of n control points P_a, where $P_a \in R^d$, $1 \le a \le n$, $d = 2$ or 3.
- A knot vector U $= \{\xi_1, \xi_2, \ldots, \xi_{n+p+1}\}$.
- A set of n weights w_i, $i = 1, 2, \ldots, n$.

Then the B-spline basis functions are denoted by $N_{i,p}$ with $1 \le i \le n$ and are defined as follows for $p = 0$

$$N_{i,0} = \begin{cases} 1, & if\, \xi_i < \xi < \xi_{i+1} \\ 0, & otherwise \end{cases} \tag{15}$$

and for $p = 1, 2, 3, \ldots$:

$$N_{i,p} = \frac{\xi - \xi_i}{\xi_{i+p} - \xi_i}N_{i,p-1}(\xi) + \frac{\xi_{i+p+1} - \xi}{\xi_{i+p+1} - \xi_{i+1}}N_{i+1,p-1}(\xi) \tag{16}$$

The B-spline curve can be constructed as a linear combination of B-spline basis functions and control points, being

$$\mathbf{X}(\xi) = \sum_{i=1}^{n} N_{i,p}(\xi)\mathbf{P}_i \tag{17}$$

where the coefficients $\mathbf{P}_i$ denotes the coordinates of control points and $\mathbf{X} = (x, y)$ is the location of the physical space corresponding to the spatial coordinate ξ parametric space.

NURBS are the extension of B-spline by assigning a positive weight ω_i to each basis function:

$$\mathbf{X}(\xi) = \sum_{i=1}^{n} R_{i,p}(\xi)\mathbf{P}_i \tag{18}$$

where $R_{i,p}(\xi)$ with local coordinate ξ is defined as follows:

$$R_{i,p}(\xi) = \frac{N_{i,p}(\xi)w_i}{W(\xi)} \tag{19}$$

with

$$W(\xi) = \sum_{i=1}^{n} N_{i,p}(\xi)\omega_i \tag{20}$$

The NURBS surface is defined using NURBS basis functions and referred control points under same manner as B-spline surface, and it is the extension of NURBS, being

$$\mathbf{X}(\xi,\eta)=\sum_{i=1}^{n}\sum_{j=1}^{m}R_{i,p}(\xi)R_{j,q}(\eta)\mathbf{P}_{i,j} \tag{21}$$

If all the weights are equal to one, NURBS surface can be degenerated as B-spline surface. For the simplicity, in the following the geometries in isogeometric analysis can be described using global index A.

$$\mathbf{X}(\mathbf{s})=\sum_{A=1}^{N_A}R_A(\mathbf{s})\mathbf{P}_A \tag{22}$$

where $\mathbf{s}$ denotes the vector form of spatial coordinates in parametric space, hence $\mathbf{s}=\xi$ in 2D problems and $\mathbf{s}=(\xi,\eta)$ in 3D problems. Generally, the geometry and fields are described by the same NURBS basis functions in isogeometric analysis (IGA), then the displacements and tractions on the interface in Eq. (1) can be given as

$$\mathbf{u}(\mathbf{s})=\sum_{A=1}^{N_A}R_A(\mathbf{s})\mathbf{d}_A \tag{23}$$

and

$$\mathbf{t}(\mathbf{s})=\sum_{A=1}^{N_A}R_A(\mathbf{s})\mathbf{q}_A \tag{24}$$

in which $\mathbf{d}_A$ and $\mathbf{q}_A$ are the related displacement and traction vectors corresponding to Ath control point according to global index. But they have not specific physical meanings. $\mathbf{u}$ and $\mathbf{t}$ are the real displacements and tractions on the interface between the inclusion and matrix, respectively.

4. Isogeometric boundary element method (IGABEM)

4.1. Boundary integral equation (BIE)

In order to obtain the elastic energy increment ΔU in Eqs. (13) and (14), the traditional subdomain BEM is applied in heterogeneous problems because fundamental solutions to anisotropic structures are few or difficult to obtain, the boundary integral equation for an infinite isotropic elastic matrix subjected to remote stresses can be written as

$$c_{ki}^{M}(p)u_i^{M}(p)=u_k^{0}(p)+\int_{\Gamma}U_{ki}^{M}(p,q)t_i^{M}(q)d\Gamma(q)-\int_{\Gamma}T_{ki}^{M}(p,q)u_i^{M}(q)d\Gamma(q) \tag{25}$$

where $c_{ki}=\frac{1}{2}\delta_{ki}$ for smooth boundary and it depends on the boundary geometry of source point p. q denotes field point on the interface Γ between the inclusion and matrix. The superscript M means the material properties of the matrix, and u_k^0 denotes the variables that are generated by the remote loading on the interface Γ. The U and T denote the fundamental solutions for displacement and traction for isotropic elastic medium, i.e. for 3D problem, we have [42]

$$U_{ki}=\frac{1}{16\pi\mu(1-v)\mathrm{r}}[(3-4v)\delta_{ki}+r_{,k}r_{,i}] \tag{26}$$

and

$$T_{ki}=-\frac{1}{8\pi(1-v)r^2}[r_{,n}((1-2v)\delta_{ik}+3r_{,i}r_{,k})+(1-2v)(n_ir_{,k}-n_kr_{,i})] \tag{27}$$

where v is the Poisson' s ratio, and μ is the shear modulus as the same as G. n_i and n_k are the direction cosines of unit vector $\mathbf{n}$ with respect to x_i and x_k. And r means the distance between the source point p and field point q, respectively. $r_{,i}=\partial r(p,q)/\partial x_i(q)$ which means the derivation of r with respect to x_i.

For two dimensional (2D) plain strain problems, the kernel functions U and T are given as

$$U_{ki}=\frac{1}{8\pi\mu(1-v)}[(3-4v)\ln\frac{1}{r}\delta_{ki}+r_{,k}r_{,i}] \tag{28}$$

and

$$T_{ki}=-\frac{1}{4\pi(1-v)r}[r_{,n}((1-2v)\delta_{ik}+2r_{,i}r_{,k})+(1-2v)(n_ir_{,k}-n_kr_{,i})] \tag{29}$$

Note that the kernel function of U is weak singularity and the kernel function of T is strong singularity. In order to solve singularities of those fundamental solutions in Eqs. (26) and (27), the so-called Telles algorithm [38] is used,

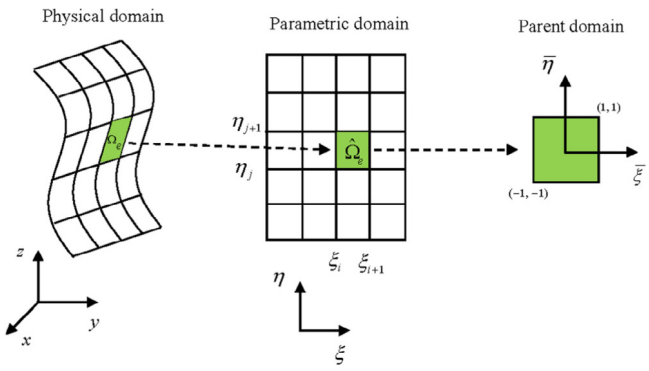

Fig. 2. Definition of domains in isogeometric analysis.

which allows to remove the singularity by a local change of coordinates. Meanwhile, for Eqs. (28) and (29), in order to eliminate the singularities in 3D IGABEM, the power series expansion method is employed [26], in which a surface integral is divided into a line integral over contour of the integration surface and a radial integral containing the singularities. The singularities condensed in the radial integral are removed analytically or numerically by extracting the finite value parts from the power series expansion.

The boundary integral equation from the inclusion part can be written as

$$c_{ki}^{I}(p)u_i^{I}(p) = \int_{\Gamma} U_{ki}^{I}(p,q)t_i^{I}(q)d\Gamma(q) - \int_{\Gamma} T_{ki}^{I}(p,q)u_i^{I}(q)d\Gamma(q) \tag{30}$$

where all meanings of the symbols are similar to those in Eq. (25), the superscript I denotes the inclusion part. It is worth noting that the integral directions are reverse between the interface from the matrix and from the inclusion.

4.2. Isogeometric approximate

In the conventional BEM, the interface Γ is discretized into E elements, i.e.

$$\Gamma = \bigcup_{e=1}^{E} \Gamma_e \tag{31}$$

Then, the boundary integral equations in (25) and (30) in 3D problems can be converted as

$$c_{ki}^{M}(p)u_i^{M}(p) = u_k^{0}(p) + \sum_{e=1}^{E}\int_{\Gamma_e} U_{ki}^{M}(p,q)t_i^{M}(q)d\Gamma(q) - \sum_{e=1}^{E}\int_{\Gamma_e} T_{ki}^{M}(p,q)u_i^{M}(q)d\Gamma(q) \tag{32}$$

and

$$c_{ki}^{I}(p)u_i^{I}(p) = \sum_{e=1}^{E}\int_{\Gamma_e} U_{ki}^{I}(p,q)t_i^{I}(q)d\Gamma(q) - \sum_{e=1}^{E}\int_{\Gamma_e} T_{ki}^{I}(p,q)u_i^{I}(q)d\Gamma(q) \tag{33}$$

Unlike the conventional BEM, the NURBS basis functions in IGABEM are chosen to exactly describe the geometry, and in the concept of IGA, those functions are also applied on describing the distribution of unknown fields as shown in Eqs. (23) and (24). In order to carry out numerical integration by Gauss–Legendre quadrature, local coordinates $\bar{\xi}$ and $\bar{\eta}$ must be in the range of $[-1, 1]$. Therefore, there should be a transformation from the parameter space $(\xi, \eta) \in [\xi_i, \xi_{i+1}] \times [\eta_j, \eta_{j+1}]$ to the parent space $(\bar{\xi}, \bar{\eta}) \in [-1, 1] \times [-1, 1]$. Fig. 2 illustrates the relationship between physical domain Ω_e, parameter domain $\hat{\Omega}_e$ and parent domain. After substituting the displacements and tractions in Eqs. (32) and (33) into Eqs. (23) and (24), we can obtain the boundary integral equations in IGABEM as follows

$$c_{ki}^{M}(\mathbf{s}_p)\sum_{A=1}^{N_A} R_A(\mathbf{s}_p)d_{Ai}^{M} = u_k^{0}(\mathbf{s}_p) + \sum_{e=1}^{E}\sum_{A=1}^{N_A} P_{eA}^{M}(\mathbf{s}_p,\mathbf{s}_q)q_{Ai}^{M} - \sum_{e=1}^{E}\sum_{A=1}^{N_A} Q_{eA}^{M}(\mathbf{s}_p,\mathbf{s}_q)d_{Ai}^{M} \tag{34}$$

where

$$P_{eA}^{M}(\mathbf{s}_p,\mathbf{s}_q) = \int_{\mathbf{s}_i}^{\mathbf{s}_{i+1}} U_{ki}^{M}(\mathbf{s}_p,\mathbf{s}_q)R_A(\mathbf{s}_q)J d\mathbf{s} \tag{35}$$

$$Q_{eA}^{M}(\mathbf{s}_p,\mathbf{s}_q) = \int_{\mathbf{s}_i}^{\mathbf{s}_{i+1}} T_{ki}^{M}(\mathbf{s}_p,\mathbf{s}_q)R_A(\mathbf{s}_q)J d\mathbf{s} \tag{36}$$

and for the inclusion part,

$$c_{ki}^{I}(\mathbf{s}_p)\sum_{A=1}^{N_A} R_A(\mathbf{s}_p)d_{Ai}^{I} = \sum_{e=1}^{E}\sum_{A=1}^{N_A} P_{eA}^{I}(\mathbf{s}_p,\mathbf{s}_q)q_{Ai}^{I} - \sum_{e=1}^{E}\sum_{A=1}^{N_A} Q_{eA}^{I}(\mathbf{s}_p,\mathbf{s}_q)d_{Ai}^{I} \tag{37}$$

where

$$P_{eA}^{I}(\mathbf{s}_p,\mathbf{s}_q) = \int_{\mathbf{s}_i}^{\mathbf{s}_{i+1}} U_{ki}^{I}(\mathbf{s}_p,\mathbf{s}_q)R_A(\mathbf{s}_q)J d\mathbf{s} \tag{38}$$

$$Q_{eA}^{I}(\mathbf{s}_p,\mathbf{s}_q) = \int_{\mathbf{s}_i}^{\mathbf{s}_{i+1}} T_{ki}^{I}(\mathbf{s}_p,\mathbf{s}_q)R_A(\mathbf{s}_q)J d\mathbf{s} \tag{39}$$

in which J means the Jacobian of transformation from the physical domain to parametric domain, for example, in 3D problems, it is given as

$$J = [(\frac{\partial x_2}{\partial \xi}\frac{\partial x_3}{\partial \eta} - \frac{\partial x_3}{\partial \xi}\frac{\partial x_2}{\partial \eta})^2 + (\frac{\partial x_3}{\partial \xi}\frac{\partial x_1}{\partial \eta} - \frac{\partial x_1}{\partial \xi}\frac{\partial x_3}{\partial \eta})^2 + (\frac{\partial x_1}{\partial \xi}\frac{\partial x_2}{\partial \eta} - \frac{\partial x_2}{\partial \xi}\frac{\partial x_1}{\partial \eta})^2] \tag{40}$$

and $\mathbf{s}_p$ and $\mathbf{s}_q$ denote the collocation points corresponding to source point p and field point q. In the concept of IGA, the collocation points are obtained by the Greville abscissae definition [44], which are defined as

$$\xi_i' = (\xi_{i+1} + \xi_{i+2} + \cdots + \xi_{i+p})/p \quad i = 1, 2, \ldots, n \tag{41}$$

$$\eta_j' = (\eta_{j+1} + \eta_{j+2} + \cdots + \eta_{j+q})/q \quad j = 1, 2, \ldots, m \tag{42}$$

where n and m are the number of control points along ξ and η directions. p and q are the orders of the curves along and directions, respectively.

In order to deal with corner point problem in heterogeneous structure, discontinuous element method is implemented in IGABEM, the improved Greville abscissae method (with coefficient $\beta = 0.5$) moves the first and last collocation points inside the patch by

$$\xi_1' = \xi_1' + \beta(\xi_2' - \xi_1') \tag{43}$$

$$\xi_n' = \xi_1' - \beta(\xi_n' - \xi_{n-1}') \tag{44}$$

and more details of that can be found in [45].

Loop the source point p and calculate all the integrals in Eqs. (34) and (37), we can obtain the global system equations in matrix form, i.e.

$$\mathbf{H}^M\mathbf{d}^M = \mathbf{u}^0 + \mathbf{G}^M\mathbf{q}^M \tag{45}$$

$$\mathbf{H}^I\mathbf{d}^I = \mathbf{G}^I\mathbf{q}^I \tag{46}$$

where $\mathbf{d}$ and $\mathbf{q}$ are vectors containing the displacement and traction nodal parameters on control points, $\mathbf{u}^0$ is the vector of displacement derived from remote loading. M and I denote the matrix part and the inclusion part, respectively. $\mathbf{H}$ and $\mathbf{G}$ are the corresponding coefficient matrixes, whose entries are given as follows

$$H_{ki} = c_{ki}(\mathbf{s}_p)\sum_{A=1}^{N_A} R_A(\mathbf{s}_p) + \sum_{e=1}^{E}\sum_{A=1}^{N_A} Q_{eA}(\mathbf{s}_p,\mathbf{s}_q) \tag{47}$$

and

$$G_{ki} = \sum_{e=1}^{E}\sum_{A=1}^{N_A} P_{eA}^{M}(\mathbf{s}_p,\mathbf{s}_q) \tag{48}$$

Note that there are same displacement and adverse traction on the identical collocation point on the interface between the matrix and inclusion, which are called displacement continuous and traction balance conditions $\mathbf{u}^M = \mathbf{u}^I, \mathbf{t}^M = -\mathbf{t}^I$. Meanwhile, these conditions are satisfied on control points, i.e.

$$\mathbf{d}^M = \mathbf{d}^I, \mathbf{q}^M = -\mathbf{q}^I \tag{49}$$

Combined with displacement continuous and traction balance conditions in Eq. (49), the displacement can be solved from Eqs. (45) and (46) by the following equation

$$(\mathbf{H}^M + \mathbf{G}^M(\mathbf{G}^I)^{-1}\mathbf{H}^I)\mathbf{d}^M = \mathbf{u}^0 \tag{50}$$

However, due to the opposite integral directions mentioned in Eqs. (25) and (30), the global index A in coefficient matrixes $\mathbf{H}^I$ and $\mathbf{G}^I$ for the inclusion part must be converted into the same as that in coefficient matrix $\mathbf{H}^M$ and $\mathbf{G}^M$. Assumed that the global index for the matrix part is $A = (i-1)m + j$, then the global index for the inclusion part is $A = (n-i)m + j$ as shown in Fig. 3.

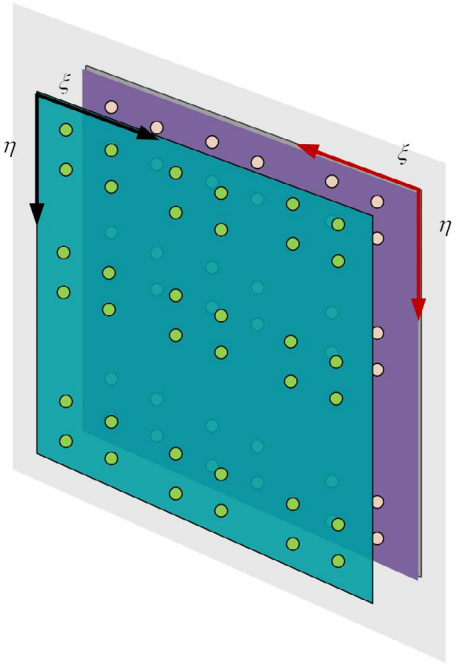

Fig. 3. Comparison of the element between double layers in parametric space.

By substituting the displacement in Eq. (50) into the new integral formula in Eq. (13), the process of calculating interfacial tractions is avoided, and the elastic energy increment of heterogeneous structure can be obtained effectively.

5. Evaluation of singular boundary integrals

In the implementation of IGABEM, the numerical accuracy evaluation of singular integrals is the crucial and difficult point. Gauss–Legendre quadrature is the traditional and more accurate method to calculate regular integrals. However, when some kinds of singular integrals appear, such as weakly singular, strongly singular or hypersingular, the accuracy and stability of the integrals will be lost. In order to solve these problems, many methods have been provided. Simpson et al. [24,25] used Subtraction of Singularity Method (SST) and Telles transformation [38] to evaluate the strongly and weakly singular integrals appearing in 2D IGABEM, respectively. In order to eliminate the singularities in 3D IGABEM, the power series expansion method is employed [26], in which a surface integral is divided into a line integral over contour of the integration surface and a radial integral containing the singularities. The singularities condensed in the radial integral are removed analytically or numerically by extracting the finite value parts from the power series expansion.

Consider eth element in Eqs. (34) and (37) as shown in Fig. 4, X is the source point locating on the edge or domain of this element, and the singular integral is formulated in parametric space as

$$I^e(X) = \int_{S_e} \frac{\bar{f}(X,Y)}{r^{\lambda}(X,Y)} dS = \int_{-1}^{1}\int_{-1}^{1} \frac{\bar{f}(X,Y)}{r^{\lambda}(X,Y)} J_e d\xi\, d\eta \tag{51}$$

in which λ denotes the order of singularity of fundamental solution, J_e is the Jacobian of the transformation from the parametric domain to the parent domain. $\bar{f}$ is the nonsingular part of BIE, and we rewrite it using linear integral around the edge of element, i.e.

$$I^e(X) = \int_L \frac{1}{\rho(X,Y)} \frac{\partial \rho(X,Y)}{\partial \mathbf{n}_L} F(X,Y) dL \tag{52}$$

where $\mathbf{n}_L$ is the outer normal vector of square sides, and

$$F(X,Y) = \lim_{\rho_\alpha(\varepsilon)\to 0} \int_{\rho_\alpha(\varepsilon)}^{\rho(\mathbf{X},\mathbf{Y})} \frac{\bar{f}(x,X)}{r^{\lambda}(x,X)} J_e \rho d\rho \tag{53}$$

in which ρ is the distance in parametric space between source point X and selected point x, and it is defined as

$$\rho = \sqrt{(\xi - \xi_p)^2 + (\eta - \eta_p)^2} \tag{54}$$

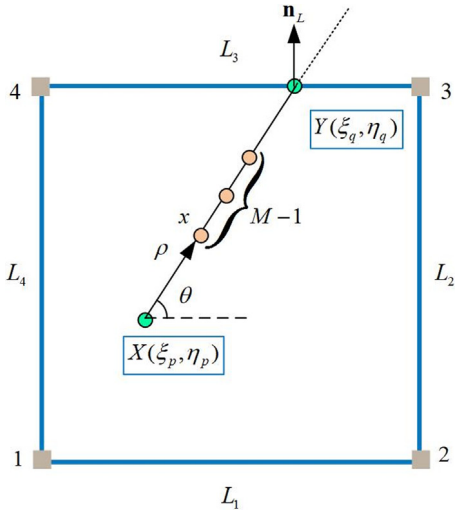

Fig. 4. Integral element in parametric domain.

Table 1
The values of the power M.

N_{node}	4	8	9
M	2	4	6

Obviously, the local coordinates ξ and η can be represented by ρ,

$$\begin{cases} \xi = \xi_p + \rho\cos\theta \\ \eta = \eta_p + \rho\sin\theta \end{cases} \tag{55}$$

In order to degenerate the singularity, we reformulate the distance by radius expansion as

$$\frac{r}{\rho} = (\sum_{m=0}^{M} G_m \rho^m)^{1/2} = \sum_{n=0}^{N} C_n \rho^n \tag{56}$$

where $(M-1)$ is the total number of interpolation points between X and Y, and G_m can be expressed as

$$\mathbf{R}(M)\mathbf{G} = \mathbf{Z} \tag{57}$$

in which

$$\begin{aligned} Z_m &= [(r_i/\rho_i)^2 - G_0]/\rho_i, \\ R_m &= [1\rho_m \cdots \rho_m^{M-1}], \end{aligned} \quad m = 1, 2, \ldots, M \tag{58}$$

and

$$G_0 = \lim_{\rho\to 0}(\frac{r}{\rho})^2 = \left|\frac{\partial \mathbf{r}}{\partial \xi}\rho_{,\xi} + \frac{\partial \mathbf{r}}{\partial \eta}\rho_{,\eta}\right| \tag{59}$$

Table 1 gives the values of M for different nodes of each element.

We derive the radius integral by power series form of ρ, which is expressed as

$$F(X,Y) = \sum_{k=0}^{K} B^{(k)} \lim_{\rho_\alpha(\varepsilon)\to 0} \int_{\rho_\alpha(\varepsilon)}^{\rho(X,Y)} \rho^{k-\lambda+1} d\rho = \sum_{k=0}^{K} B^{(k)} E_k \tag{60}$$

where

$$E_k = \begin{cases} \dfrac{1}{k-\lambda+2}[\dfrac{1}{\rho^{\lambda-k-2}(X,Y)} - \lim\limits_{\rho_\alpha(\varepsilon)\to 0} \dfrac{1}{\rho_\alpha^{\lambda-k-2}(\varepsilon)}], & k \neq \lambda-2 \\ \ln\rho(X,Y) - \lim\limits_{\rho_\alpha(\varepsilon)\to 0} \ln\rho_\alpha(\varepsilon), & k = \lambda-2 \end{cases} \tag{61}$$

Extracting the limiting part from finite part of Eq. (61), which can be reformulated to the sum of finite and infinite part as

$$\begin{cases} \lim\limits_{\rho_s \to 0} \ln \rho_s(\varepsilon) = \ln H_0 + \infty, \\ \lim\limits_{\rho_s \to 0} \dfrac{1}{\rho_s^{\lambda-k-1}(\varepsilon)} = H_{\lambda-k-1} + \infty, \quad 0 \le k \le \lambda - 2 \end{cases} \tag{62}$$

where

$$\begin{cases} H_0 = 1/C_0; H_1 = \overline{C}_1; H_2 = 2\overline{C}_2 - \overline{C}_1^2 \\ H_3 = 3\overline{C}_3 - 3\overline{C}_1\overline{C}_2 + \overline{C}_1^2; \\ H_4 = 4\overline{C}_4 + 4\overline{C}_1^2\overline{C}_2 - 4\overline{C}_1\overline{C}_2 - 2\overline{C}_2^2 - \overline{C}_1^4 \end{cases} \tag{63}$$

in which $\overline{C}_i = C_i/C_0$.

There are definite results of numerical integrals for a practical physical problem, in other words, the infinitesimal part of Eq. (61) tends to zero when the radius distance goes to zero, thus Eq. (61) can be rewritten as

$$E_k = \begin{cases} \dfrac{1}{k-\lambda+2}[\dfrac{1}{\rho^{\lambda-k-2}(X,Y)} - H_{\lambda-k-2}], & 0 \le k \le \lambda - 3 \\ \ln \rho(X,Y) - \ln H_0, & k = \lambda - 2 \\ \dfrac{\rho^{k-\lambda+2}(X,Y)}{k-\lambda+2}, & k > \lambda - 2 \end{cases} \tag{64}$$

For hypersingular integral in 2D problems, the singular order λ is up to 5. Meanwhile, this power series expansion method can be used to solve hypersingular integral whose order is up to 6 in 3D problems.

6. Numerical examples

In this section, several numerical examples are given to verify the accuracy and effectiveness of the proposed method. The solution procedure for numerical computation is implemented using Fortran 95 under Intel® Core™ i7-8550 CPU @ 1.80 GHz. In order to confirm the accuracy and convergence of the proposed method, the relative error is defined as:

$$\varepsilon_r = \left| \frac{I_{num} - I_{ref}}{I_{ref}} \right| \tag{65}$$

where I_{num} and I_{ref} denote the numerical and reference values of the change of elastic strain energy.

All the geometries are modeled by NURBS basis functions.

6.1. Cylindrical inclusion in an infinite matrix

One cylindrical inclusion with radius $a = 3$ m, as shown in Fig. 5, is embedded in an infinite isotropic matrix subjected to remote loading $\sigma_{xx}^0 = \sigma_{yy}^0 = \sigma^0$. The accuracy and effectiveness of the new integral formula combined with IGABEM are analyzed. The analytical solution of variation of elastic energy of heterogeneous materials can be derived easily by the well-known elasticity [46], i.e.

$$\Delta U = \pi \sigma^0 a u_r (1 - \frac{(1+v_M)E_I}{(1+v_I)E_M} - 2\frac{(v_I - v_M)(1+v_M)E_I}{(1+v_I)(1-2v_I)E_M}) \tag{66}$$

where

$$u_r = \frac{\sigma^0 a(1-v_M)}{\mu_M}(\frac{1-2v_I}{1-2v_I+\mu_I/\mu_M}) \tag{67}$$

In numerical computation, uniform bidirectional stress is $\sigma^0 = 10^4$ Mpa, the material properties for the matrix part are $E_M = 10^4$ Mpa, $v_M = 0.3$ and those for the inclusion part are $E_I = 2 \times 10^4$ Mpa, $v_I = 0.3$. The matrix-inclusion interface is meshed by NURBS, in which the knot vector is U = {0, 0, 0, 1, 1, 2, 2, 3, 3, 4, 4, 4}, the weights are $w = [1, \sqrt{2}/2, 1, \sqrt{2}/2, 1, \sqrt{2}/2, 1, \sqrt{2}/2, 1]$ and the order of NURBS basis functions is $p = 2$. We use Subtraction of Singularity Method (SST) and Telles transformation [25] to deal with singular integrals in Eqs. (45) and (46). In Fig. 6, the number of Gauss quadrature points in the regular integral is set to 20, and the relative error of elastic energy increment reduces to 10^{-8} when the number of Gauss quadrature points for singular integral is set to be 8. In the following sections about 2D problems, the numbers of Gauss quadrature points for the regular and the singular integrals are set to 8 and 10, respectively. Fig. 7 gives the relative errors of elastic energy increment and the relationship between the increment and the dimensionless quantity E_I/EM, in which the number of degrees of freedom is 48.

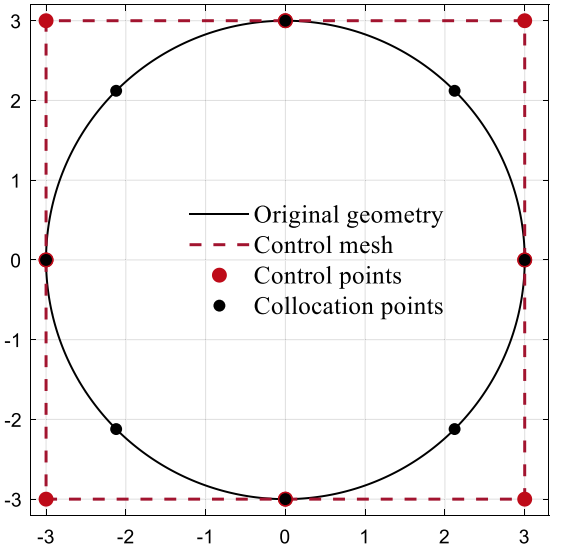

Fig. 5. Single circular inclusion under bidirectional stresses.

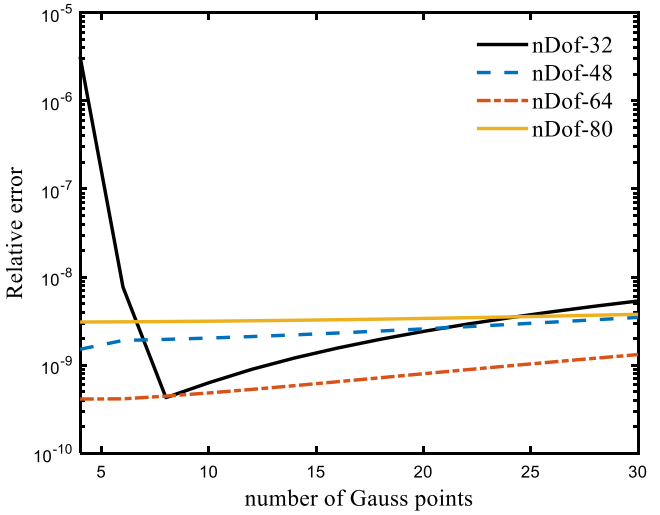

Fig. 6. The relative errors of elastic energy increment. The numbers of degrees of freedom (nDof) are obtained from four different *h*-refinement times.

6.2. Complex shape inclusion in an infinite matrix

In this section, a complex shape inclusion with the key geometric parameter $a = 3$ m as shown in Fig. 8 is embedded in an infinite isotropic matrix subjected to remote loading $\sigma^0_{xx} = \sigma^0_{yy} = \sigma^0 = 10^4$ Mpa, and the material properties of the heterogeneous structure are the same as the above example. Fig. 8 shows that four classes of meshes, in which the order of NURBS is $p = 2$ and the control points and related weights in Fig. 8(a) are given in Table 2. One can observe from Fig. 9 that the results of ΔU from four classes of meshes are quite consistent with each other. When considering different Poisson's ratios for the matrix and inclusion parts, Fig. 10 gives the relationships between the variations of elastic energy ΔU and the dimensionless quantity E_I/EM under various Poisson's ratios of the inclusion part.

6.3. Spherical inclusion in 3D infinite matrix

One spherical inclusion with radius $a = 1$ m as shown in Fig. 11 is embedded in an 3D infinite isotropic matrix subjected to remote loading $\sigma^0_{xx} = \sigma^0_{yy} = \sigma^0_{zz} = \sigma^0 = 10^4$ Mpa and the material properties of the heterogeneous structure are the same as the first example. The analytical solution of variation of elastic energy of heterogeneous materials can be

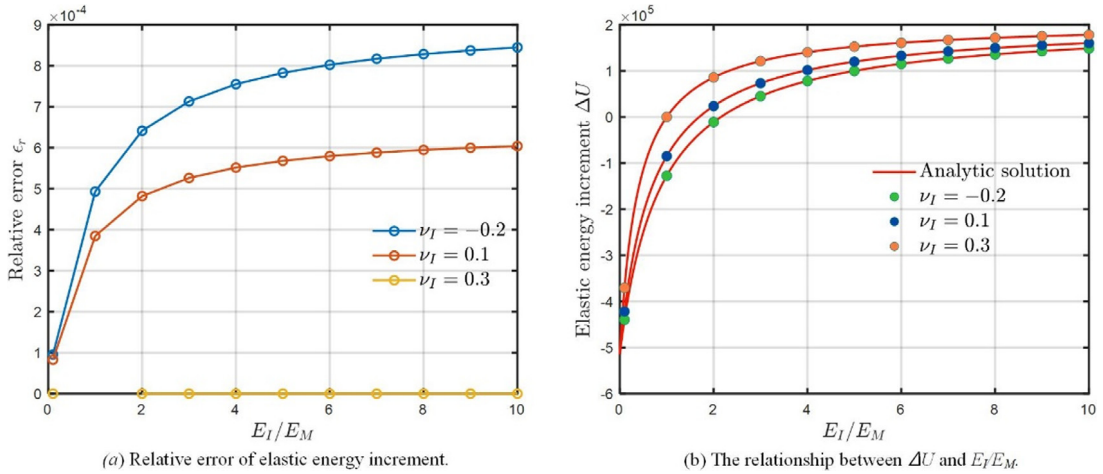

Fig. 7. The comparison between the numerical and analytical results of elastic energy increment.

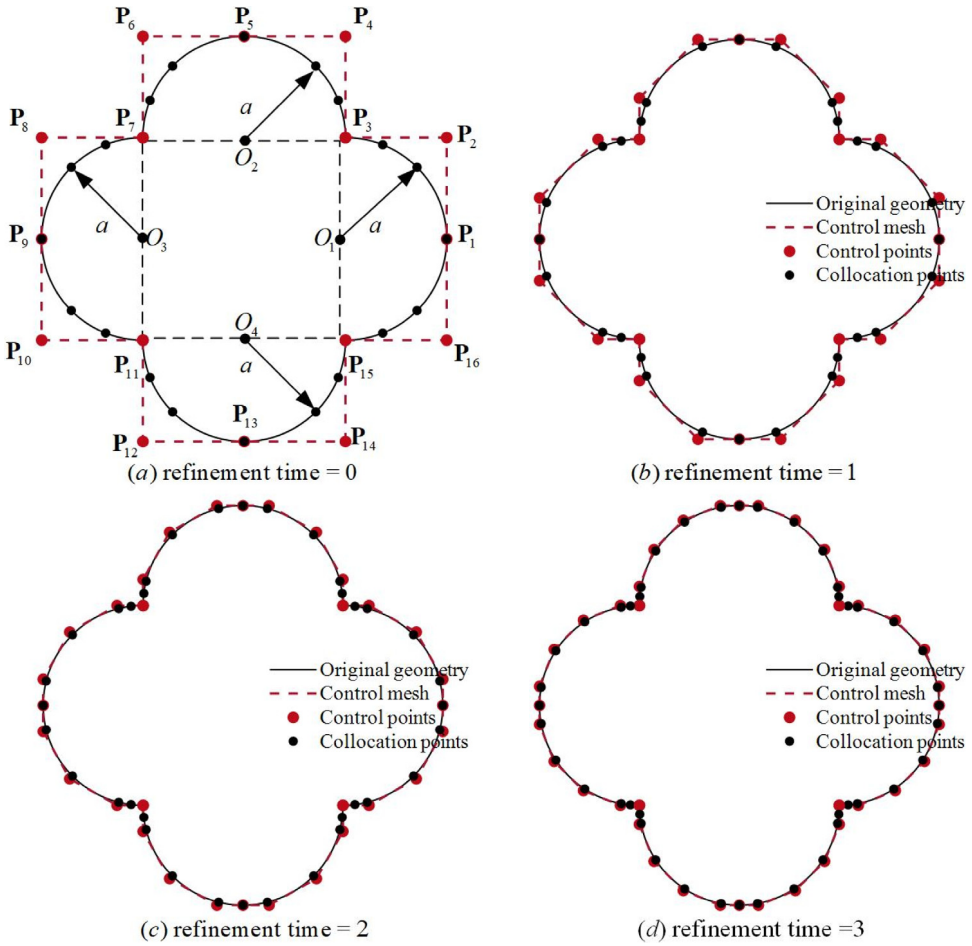

Fig. 8. The isogeometric model of the interface between the matrix and inclusion.

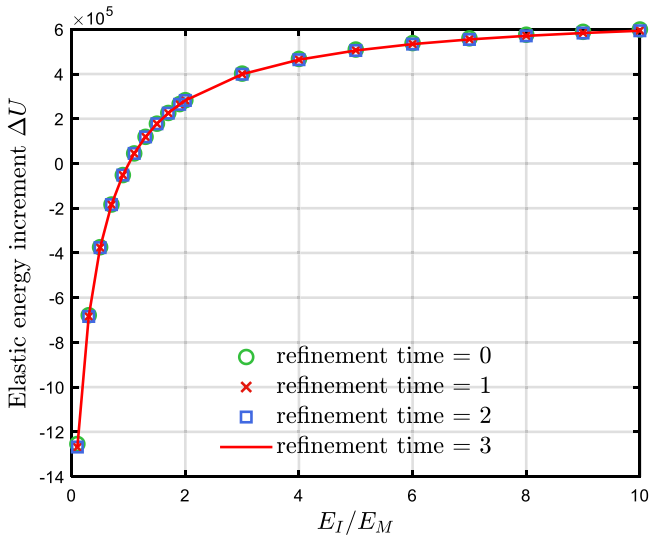

Fig. 9. The elastic energy increment caused by the 2D complex shape inclusion.

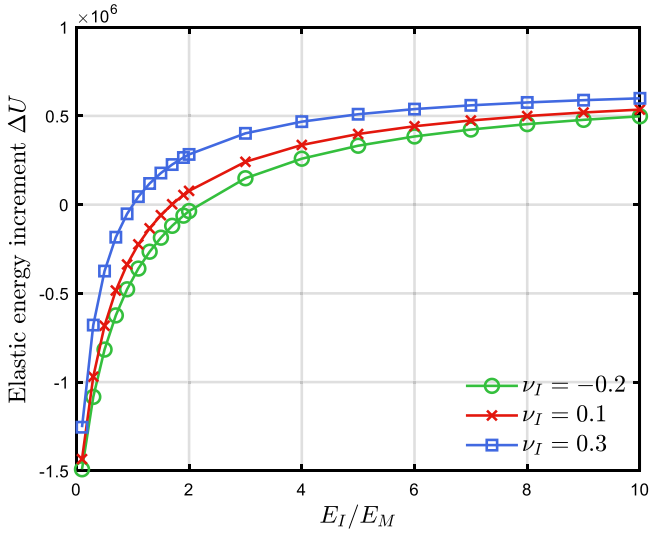

Fig. 10. The various variations of elastic energy of heterogeneous materials under different Poisson's ratios of the inclusion v_I.

deduced easily by the well-known elasticity [46] as follows:

$$\Delta U = 2\pi a^2 \sigma^0 u_r (1 - \frac{(1+v_M)E_I}{(1+v_I)E_M} - 3\frac{(v_I - v_M)(1+v_M)E_I}{(1+v_I)(1-2v_I)E_M}) \tag{68}$$

where

$$u_r = \frac{1.5a\sigma^0(1-2v_I)(1-v_M)}{0.5(1+v_M)E_I + (1-2v_I)E_M} \tag{69}$$

in which u_r denotes the radial displacement on the interface between the matrix and inclusion.

Since the accuracy of the proposed method is mainly affected by the number of Gauss quadrature points and the degrees of freedom, the corresponding convergence studies are performed to better understand the performance of the proposed method. Fig. 12 shows that the relative error between the numerical and analytical results decreases with the increase of degrees of freedom and number of Gauss quadrature points, locating in each line integral over contour of the integration surface, for singular integration. The error first decreases rapidly and then converges as Gauss quadrature

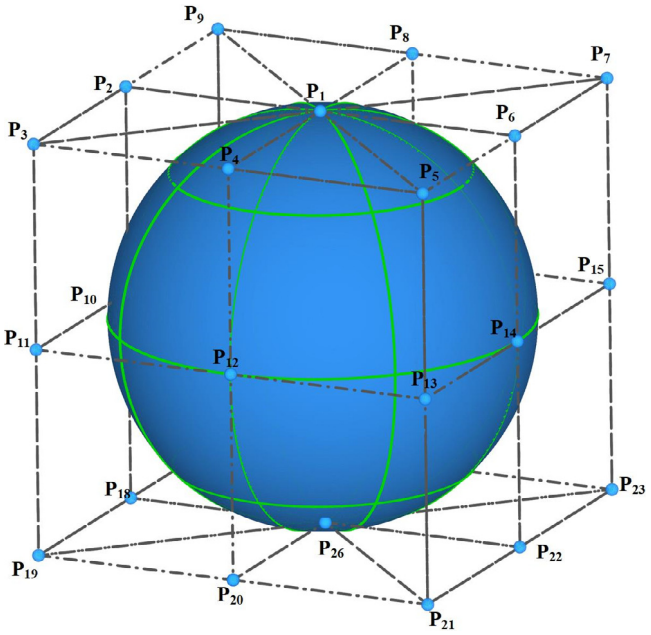

Fig. 11. The two knot vectors for NURBS surface are U = {0, 0, 0, 1, 1, 2, 2, 3, 3, 4, 4, 4} and V = {0, 0, 0, 1, 1, 2, 2, 2}. Degree 2 is chosen in both directions. This NURBS surface can be divided into 8 patches according to the continuity of knot vector. The numbers of elements and control points are 8 and 26. The coordinates of control points are (0, 0, 1) for $\mathbf{P_1}$, (1, 1, 0) for $\mathbf{P_{11}}$ and (0, 0, −1) for $\mathbf{P_{26}}$.

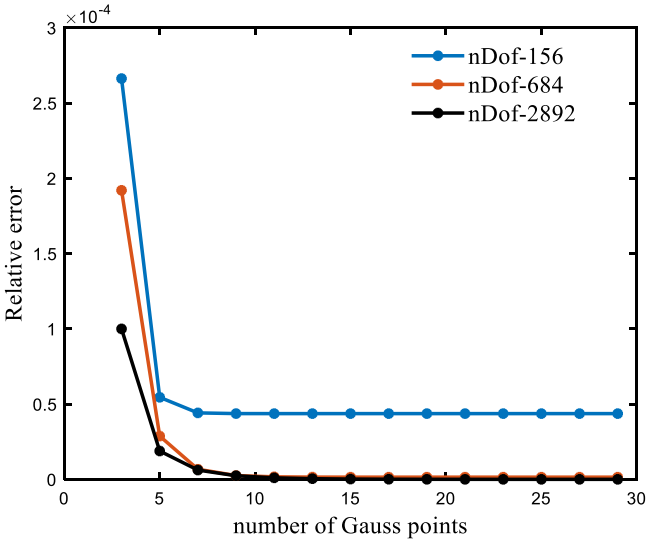

Fig. 12. The relative error in terms of Gauss point for the singular integration when the number of Gauss points for the regular integration is equal to 20. The numbers of degrees of freedom (nDof) are obtained from three different *h*-refinement times. The coordinate on *x*-axis means the number of Gauss points, i.e. 8 in *x*-axis denotes 8×8 Gauss points.

points increase. For both accuracy and efficiency, we choose 8×8 Gauss points for regular boundary integration and 10×10 Gauss points for singular boundary integration in the following 3D examples. Fig. 13 plots the relative error and CPU-time in terms of the degrees of freedom. Compared to conventional BEM based on Lagrange polynomials, the NURBS basis functions in IGABEM improve the accuracy of physical fields, but consume more computation times with identical nDof. Fig. 14 gives the comparison of elastic energy increment ΔU between the numerical and analytical results in terms of E_I/EM, in which the number of degrees of freedom is 684.

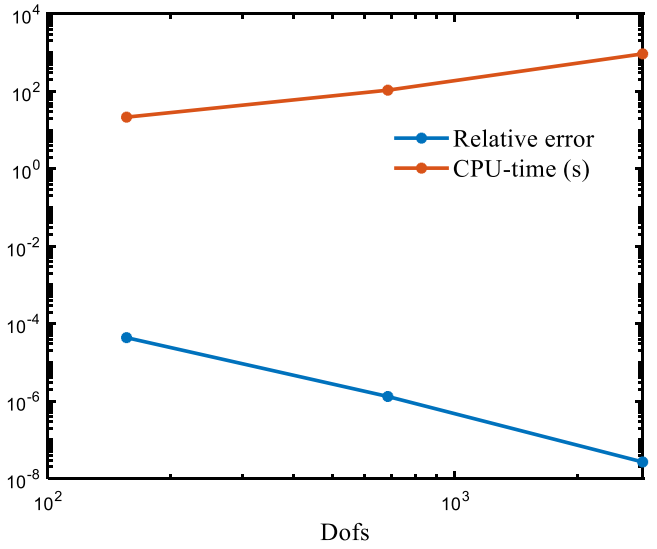

Fig. 13. The relative error and CPU-time in terms of the degrees of freedom.

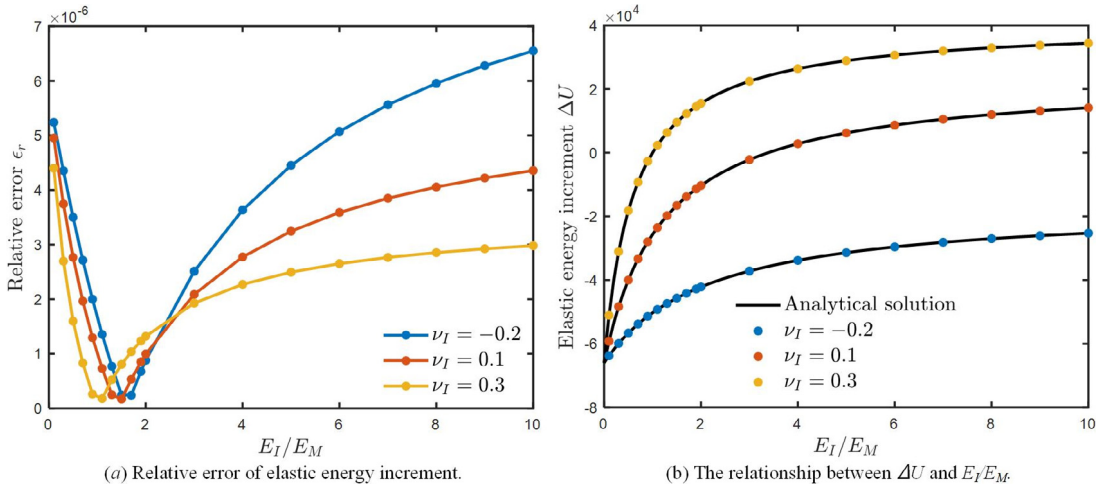

(a) Relative error of elastic energy increment. (b) The relationship between ΔU and E_I/E_M.

Fig. 14. The comparison between the numerical and analytical results of elastic energy increment.

6.4. Complex shape inclusion in 3D infinite matrix

Consider one complex shape inclusion embedded in an 3D infinite isotropic matrix subjected to remote loading $\sigma^0_{xx} = \sigma^0_{yy} = \sigma^0_{zz} = \sigma^0 = 10^4$ Mpa, and the material parameters of the heterogeneous structure are the same as the first example. In Fig. 15, the initial isogeometric model is constructed using a quadratic NURBS surface with 90 control points. The refined isogeometric model as shown in Fig. 16 is obtained from Fig. 15 by one time of h-refinement. The results from the initial model and refined model are excellent agreement with each other as shown in Fig. 17.

7. Conclusion

A more general interface integral formula for the variations of elastic energy of heterogeneous structure has been proposed, in which only displacement is the unknown field variable and without the limitation about identical Poisson's ratios for the matrix and inclusion parts. The main advantage of the algorithms is the ability of IGABEM to simulate infinite domain problem and its seamless integration with the new interface integral formula. To avoid corner point problem in heterogeneous structure, the discontinuous element method combined with IGABEM has been implemented in numerical

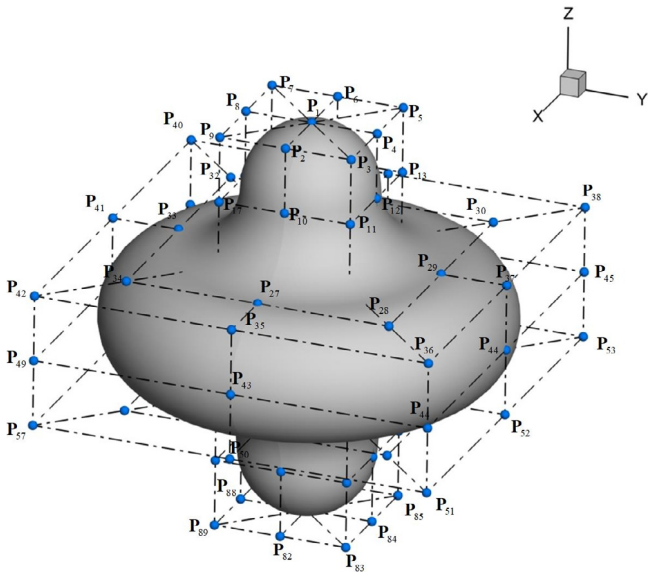

Fig. 15. Initial mesh and geometry described by NURBS. Degrees of the NURBS surface are $p = 2$ and $q = 2$ and the two corresponding knot vectors are U = {0, 0, 0, 1, 1, 2, 2, 3, 3, 4, 4, 4} and V = {0, 0, 0, 1, 1, 2, 2, 3, 3, 4, 4, 5, 5, 6, 6, 6}. The number of control points and elements are 90 and 24. The coordinates of control points are (0, 0, 30) for $\mathbf{P_1}$, (30, 0, 0) for $\mathbf{P}_{43}$ and (10, 0, 20) for $\mathbf{P}_{10}$.

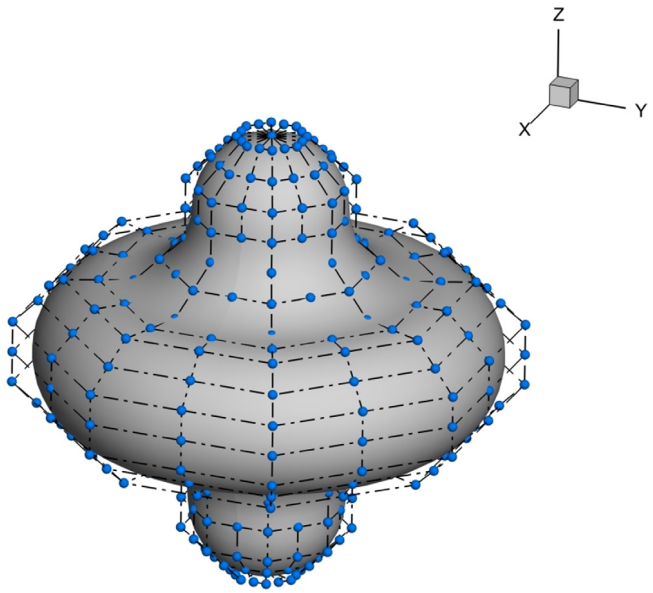

Fig. 16. Refined mesh and geometry described by NURBS. The number of control points and elements are 370 and 96. Degrees for two directions are equal to 2.

computations. In 3D numerical examples, the power series expansion method is applied to deal with strongly singular integration in boundary integral equations, and its accuracy and efficiency are shown in Fig. 13. However, this work is not without limitations, the high computation cost due to full-rank matrix hurdles its widely engineering applications. In order to improve efficiency, various methods are adapted to the BEM acceleration algorithms, including Fast Multipole Method (FMM) [47], the wideband FMM [48], Adaptive Cross Approximation (ACA) [49], etc. Moreover, the work in this paper can be further extended to the optimization of the inclusion shape and effective mechanical properties of composite materials.

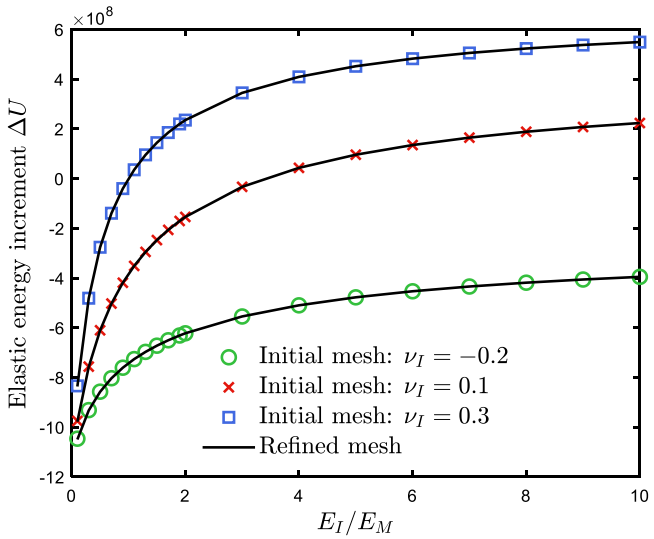

Fig. 17. The elastic energy increment caused by the 3D complex inclusion.

Table 2
The control points and weights of the complex shape inclusion in Fig. 8(*a*).

Index	X	Y	Weight	Index	X	Y	Weight
1	6.0000	0.0000	1.0000	9	−6.0000	0.0000	1.0000
2	6.0000	3.0000	0.7071	10	−6.0000	−3.0000	0.7071
3	3.0000	3.0000	1.0000	11	−3.0000	−3.0000	1.0000
4	3.0000	6.0000	0.7071	12	−3.0000	−6.0000	0.7071
5	0.0000	6.0000	1.0000	13	0.0000	−6.0000	1.0000
6	−3.0000	6.0000	0.7071	14	3.0000	−6.0000	0.7071
7	−3.0000	3.0000	1.0000	15	3.0000	−3.0000	1.0000
8	−6.0000	3.0000	0.7071	16	6.0000	−3.0000	0.7071

Acknowledgment

The research is supported by the National Natural Science Foundation of China (11972085, 11672038).

Appendix. The control points and weights of inclusions in 2D problems

See Table 2.

References

[1] K. Otsuka, C.M. Wayman, Shape Memory Materials, Cambridge University Press, USA, 1998.
[2] J.W. Eshelby, Elastic Inclusions and Inhomogeneities, Vol. 2, 1961, pp. 87–140.
[3] S.Y. Young, T.H. Nam, Calculation of the elastic strain energy of inclusions by the Green' s function and finite element methods, 47.
[4] M.A. Hussain, S.L. Pu, J. Underwood, Strain Energy Release Rate for a Crack under Combined Mode I and Mode II, ASTM International, West Conshohocken, PA, 1974.
[5] C.H. Wu, Fracture under combined loads by maximum-energy-release-rate criterion, J. Appl. Mech. 45 (1978) 553–558.
[6] G. Labeas, T. Kermanidis, Stress multiaxiality factor for crack growth prediction using the strain energy density theory, Theor. Appl. Fract. Mech. 45 (2006) 100–107.
[7] A. Boulenouar, N. Benseddiq, M. Mazari, Strain energy density prediction of crack propagation for 2D linear elastic materials, Theor. Appl. Fract. Mech. 67–68 (2013) 29–37.
[8] R.M. Christensen, Mechanics of Composite Materials, Wiley, New York, 1979.
[9] C.Y. Dong, A new integral formula for the variation of matrix elastic energy of heterogeneous materials, J. Comput. Appl. Math. 343 (2018) 635–642.
[10] J.A. Cottrell, T.J.R. Hughes, Y. Bazilevs, Isogeometric Analysis: Toward Integration of CAD and FEA, 2009.
[11] W.A. Wall, M.A. Frenzel, C. Cyron, Isogeometric structural shape optimization, Comput. Methods Appl. Mech. 197 (2008) 2976–2988.
[12] Y. Bazilevs, I. Akkerman, Large eddy simulation of turbulent Taylor–Couette flow using isogeometric analysis and the residual-based variational multiscale method, J. Comput. Phys. 229 (2010) 3402–3414.
[13] Y. Bazilevs, I. Akkerman, D.J. Benson, G. Scovazzi, M.J. Shashkov, Isogeometric analysis of Lagrangian hydrodynamics, J. Comput. Phys. 243 (2013) 224–243.
[14] Y. Bazilevs, T.J.R. Hughes, NURBS-based isogeometric analysis for the computation of flows about rotating components, Comput. Mech. 43 (2008) 143–150.

[15] M. Dinachandra, S. Raju, Isogeometric analysis for acoustic fluid–structure interaction problems, Int. J. Mech. Sci. 131–132 (2017) 8–25.
[16] H. Wu, W. Ye, W. Jiang, Isogeometric finite element analysis of interior acoustic problems, Appl. Acoust. 100 (2015) 63–73.
[17] A. Buffa, G. Sangalli, R. Vázquez, Isogeometric analysis in electromagnetics: B-splines approximation, Comput. Methods Appl. Mech. 199 (2010) 1143–1152.
[18] C.Y. Dong, S.H. Lo, Y.K. Cheung, Stress analysis of inclusion problems of various shapes in an infinite anisotropic elastic medium, Comput. Methods Appl. Mech. 192 (2003) 683–696.
[19] V. Chivukula, J. Mousel, J. Lu, S. Vigmostad, Micro-scale blood particulate dynamics using a non-uniform rational B-spline-based isogeometric analysis, Int. J. Numer. Methods Biomed. Eng. 30 (2015) 1437–1459.
[20] Y. Bazilevs, J.R. Gohean, T.J.R. Hughes, R.D. Moser, Y. Zhang, Patient-specific isogeometric fluid–structure interaction analysis of thoracic aortic blood flow due to implantation of the Jarvik 2000 left ventricular assist device, Comput. Methods Appl. Mech. 198 (2000) 3534–3550.
[21] J. Lu, Isogeometric contact analysis: Geometric basis and formulation for frictionless contact, Comput. Methods Appl. Mech. 200 (2011) 726–741.
[22] I. Temizer, P. Wriggers, T.J.R. Hughes, Contact treatment in isogeometric analysis with NURBS, Comput. Methods Appl. Mech. 200 (2011) 1100–1112.
[23] Y. Bai, C.Y. Dong, Z.Y. Liu, Effective elastic properties and stress states of doubly periodic array of inclusions with complex shapes by isogeometric boundary element method, Compos. Struct. 128 (2015) 54–69.
[24] R.N. Simpson, S.P.A. Bordas, H. Lian, J. Trevelyan, An isogeometric boundary element method for elastostatic analysis: 2D implementation aspects, Comput. Struct. 118 (2013) 2–12.
[25] R.N. Simpson, S.P.A. Bordas, J. Trevelyan, T. Rabczuk, A two-dimensional Isogeometric Boundary Element Method for elastostatic analysis, Comput. Methods Appl. Mech. 209–212 (2012) 87–100.
[26] Y.P. Gong, C.Y. Dong, X.C. Qin, An isogeometric boundary element method for three dimensional potential problems, J. Comput. Appl. Math. 313 (2017) 454–468.
[27] R.N. Simpson, Z. Liu, Acceleration of isogeometric boundary element analysis through a black-box fast multipole method, Eng. Anal. Bound. Elem. 66 (2016) 168–182.
[28] T. Takahashi, T. Matsumoto, An application of fast multipole method to isogeometric boundary element method for Laplace equation in two dimensions, Eng. Anal. Bound. Elem. 36 (2012) 1766–1775.
[29] M.J. Peake, J. Trevelyan, G. Coates, Extended isogeometric boundary element method (XIBEM) for two-dimensional Helmholtz problems, Comput. Methods Appl. Mech. 259 (2013) 93–102.
[30] M.J. Peake, J. Trevelyan, G. Coates, Extended isogeometric boundary element method (XIBEM) for three-dimensional medium-wave acoustic scattering problems, Comput. Methods Appl. Mech. 284 (2015) 762–780.
[31] R.N. Simpson, M.A. Scott, M. Taus, D.C. Thomas, H. Lian, Acoustic isogeometric boundary element analysis, Comput. Methods Appl. Mech. 269 (2014) 265–290.
[32] B.H. Nguyen, H.D. Tran, C. Anitescu, X. Zhuang, T. Rabczuk, An isogeometric symmetric Galerkin boundary element method for two-dimensional crack problems, Comput. Methods Appl. Mech. 306 (2016) 252–275.
[33] X. Peng, E. Atroshchenko, P. Kerfriden, S.P.A. Bordas, Linear elastic fracture simulation directly from CAD: 2D NURBS-based implementation and role of tip enrichment, Int. J. Fract. 204 (2016) 1–24.
[34] A. Sutradhar, G.H. Paulino, L.J. Gray, Symmetric Galerkin Boundary Element Method, Springer, 2008.
[35] A. Aimi, M. Diligenti, M.L. Sampoli, A. Sestini, Isogemetric analysis and symmetric Galerkin BEM: A 2D numerical study, Appl. Math. Comput. 272 (2016) 173–186.
[36] A. Aimi, M. Diligenti, M.L. Sampoli, A. Sestini, Non-polynomial spline alternatives in Isogeometric Symmetric Galerkin BEM, Appl. Numer. Math. 116 (2017) 10–23.
[37] B.H. Nguyen, X. Zhuang, P. Wriggers, T. Rabczuk, M.E. Mear, H.D. Tran, Isogeometric symmetric Galerkin boundary element method for three-dimensional elasticity problems, Comput. Methods Appl. Mech. 323 (2017) 132–150.
[38] J.C.F. Telles, A self-adaptive co-ordinate transformation for efficient numerical evaluation of general boundary element integrals, Int. J. Numer. Methods Eng. 24 (1987) 959–973.
[39] X.-W. Gao, An effective method for numerical evaluation of general 2D and 3D high order singular boundary integrals, Comput. Methods Appl. Mech. 199 (2010) 2856–2864.
[40] T.J.R. Hughes, J.A. Cottrell, Y. Bazilevs, Isogeometric analysis: CAD, finite elements, NURBS, exact geometry and mesh refinement, Comput. Methods Appl. Mech. 194 (2005) 4135–4195.
[41] C.Y. Dong, A more general interface integral formula for the variation of matrix elastic energy of heterogeneous materials, in: Mechanics and Engineering – Numerical Computation and Data Analysis, Bejing, China, 2018, pp. 95–98.
[42] C. Brebbia, J. Dominguez, Boundary Elements: An Introductory Course, 1989.
[43] G. Farin, J. Hoschek, M.-S. Kim, Handbook of Computer Aided Geometric Design, 2002.
[44] F. Auricchio, L.B. Da Veiga, T.J.R. Hughes, A. Reali, G. Sangalli, Isogeometric collocation methods, Math. Models Methods Appl. Sci. 20 (2010) 2075–2107.
[45] Y.J. Wang, D.J. Benson, Multi-patch nonsingular isogeometric boundary element analysis in 3D, Comput. Methods Appl. Mech. 293 (2015) 71–91.
[46] A.K. Mal, S.J. Singh, Deformation of Elastic Solids, 1991.
[47] L. Greengard, V. Rokhlin, A fast algorithm for particle simulations, J. Comput. Phys. 73 (1987) 325–348.
[48] C.-J. Zheng, C.-X. Bi, C. Zhang, Y.-B. Zhang, H.-B. Chen, Fictitious eigenfrequencies in the BEM for interior acoustic problems, Eng. Anal. Bound. Elem. 104 (2019) 170–182.
[49] M. Bebendorf, Approximation of boundary element matrices, Numer. Math. 86 (2000) 565–589.